

Features in Dark Energy Equation of State and Modulations in the Hubble Diagram

Jun-Qing Xia¹, Gong-Bo Zhao¹, Hong Li¹, Bo Feng² and Xinmin Zhang¹

¹*Institute of High Energy Physics, Chinese Academy of Science,
P.O. Box 918-4, Beijing 100049, P. R. China and*

²*Research Center for the Early Universe(RESCEU),
Graduate School of Science, The University of Tokyo, Tokyo 113-0033, Japan
(Dated: March 20, 2022.)*

We probe the time dependence of the dark energy equation of state (EOS) in light of three-year WMAP (WMAP3) and the combination with other tentative cosmological observations from galaxy clustering (SDSS) and Type Ia Supernova (SNIa). We mainly focus on cases where the EOS is oscillating or with local bumps. By performing a global analysis with the Markov Chain Monte Carlo (MCMC) method, we find the current observations, in particular the WMAP3 + SDSS data combination, allow large oscillations of the EOS which can leave oscillating features on the (residual) Hubble diagram, and such oscillations are potentially detectable by future observations like SNAP, or even by the CURRENTLY ONGOING SNIa observations. Local bumps of dark energy EOS can also leave imprints on CMB, LSS and SNIa. In cases where the bumps take place at low redshifts and the effective EOS is close to -1 , CMB and LSS observations cannot give stringent constraints on such possibilities. However, geometrical observations like (future) SNIa can possibly detect such features. On the other hand when the local bumps take place at higher redshifts beyond the detectability of SNIa, future precise observations like Gamma-ray bursts, CMB and LSS may possibly detect such features. In particular, we find that bump-like dark energy EOS on high redshifts *might* be responsible for the localized features of WMAP on ranges $l \sim 20 - 40$, which is interesting and deserves addressing further.

PACS number(s): 98.80.Es, 98.80.Cq

I. INTRODUCTION

The three year Wilkinson Microwave Anisotropy Probe observations (WMAP3)[1, 2, 3, 4, 5] have made so far the most precise probe on the Cosmic Microwave Background (CMB) Radiations. In the fittings to a constant equation of state (EOS) of dark energy (DE) w , combinations of WMAP with other cosmological observations are in remarkable agreement with a cosmological constant (CC) except for the WMAP + SDSS combination, where $w > -1$ is favored a bit more than 1σ [1]. The measurements of the SDSS power spectrum[6, 7] in some sense make the most precise probe of the current linear galaxy matter power spectrum and will hopefully get significantly improved within the coming few years. If the preference of $w > -1$ holds on with the accumulation of cosmological observations this will also help significantly on our understandings towards dark energy. A cosmological constant, which is theoretically problematic at present[8, 9], will NOT be the source driving the current accelerated expansion and a preferred candidate would be something like quintessence[10]. On the other hand, the observations from the Type Ia Supernova (SNIa) in some sense make the only direct detection of dark energy[11, 12, 13, 14, 15, 16] and currently a combination of WMAP + SNIa or CMB + SNIa + LSS are well consistent with the cosmological constant and the preference of a quintessence-like equation state has disappeared[1]. It is noteworthy that in the combinations with the Lyman α forest Ref.[17] shows that a constant EOS $w < -1$ is preferred slightly. Moreover when one considers the observational imprints by dynamical equation of state, an EOS which gets across -1 is mildly favored by the current observations[18, 19]. Intriguingly, we are also aware that the predictions for the luminosity distance-redshift relationship from the Λ CDM model by WMAP only are in notable discrepancies with the "gold" samples reported by Riess *et al*[14]. Although the discrepancy might be due to some systematical uncertainties in the Riess "gold" sample[14], this needs to be confronted with the accumulation of the 5-year SNLS observations[16] and the ongoing SNIa projects like the Supernova Cosmology Project (SCP) and from the Supernova Search Team (SST). Alternatively, this might be due to the implications of dynamical dark energy with oscillating equation of state.

Although the temperature-temperature correlation (TT) power of WMAP3 is now cosmic variance limited up to $l \sim 400$ and the third peak is now detected, the tentative features as discovered by the first year WMAP[20, 21, 22] are still present: the low TT quadrupole and localized oscillating features on TT for $l \sim 30 - 50$ [3]. Although the signatures of glitches on the first peak as discovered by the first year WMAP have now become weak, they do exist and go beyond the limited cosmic variance[3]. While for the low WMAP TT quadrupole many authors are inclined to attribute it to cutoff primordial spectrum[23, 24], and even BEFORE the release of the first year WMAP Ref. [25] claimed oscillating primordial spectrum could lead to oscillations around the first peak of CMB TT power, similar effects *might* be due to features on dark energy rather than inflation. For example, Ref.[26] has attributed the low

quadrupole to some subtle physics of dark energy during inflation.

In the literature there have been many investigations on inflationary models with broken scale invariance[29, 30, 31, 32, 33, 34, 35]. Such features have been invoked to explain the previously observed feature at $k \sim 0.05 \text{ Mpc}^{-1}$ [36, 37, 38, 39], or even to solve the small scale problem of the CDM model [40]¹. Moreover Ref.[27] has claimed that the pre-WMAP data could not exclude a large running of the spectral index (for relevant study see also [47]), which has been somewhat dramatically confirmed by the first year WMAP and WMAP3 in combination with other observations[1, 5] except for the case with the Lyman alpha forest[17, 28]. Inflation and dark energy, both of which describe the accelerated expansion of the universe, might have some relations and Ref.[48] proposed a new picture of quintessential inflation. Ref.[49] has made an attempt trying to find such relations from the observational aspect. While oscillating primordial spectrum may be responsible for the glitches on CMB, oscillating EOS of dark energy may be helpful to solve the coincidence problem of dark energy[50, 51, 52, 53]. In Ref.[51] in the framework of Quintom[54], an attempt was carried out to unify dark energy and inflation, meanwhile solving the coincidence problem of DE.

On theoretical aspect dark energy is among the biggest problem of modern cosmology[8, 9, 55, 56, 57, 58, 59]. Dynamical dark energy models rather than the simple cosmological constant have attracted more interests in theoretical studies[60]. In cases where the mysterious component of DE is driven by scalar fields[10, 62, 63] the EOS is typically not like that by a cosmological constant, this opens a possibility for us to tell CC from scalar dark energy models with the cosmological observations. Moreover the current observations have already opened a robust window to probe the behavior of dark energy independently, and in cases when $w \neq -1$ is preferred, dynamical DE models which satisfy the observations are put forward[54, 60, 61, 63, 64, 65, 66, 67]. Given the current ambiguity on theoretical study of dark energy, in the observational probe of DE one often uses the parametrizations of EOS.

Previously in the observational probes on oscillating features of dark energy EOS Ref.[68] has made some preliminary fittings to the pre-WMAP3 data and some relevant studies have been carried out later by Refs.[53, 69]. In the present paper with the method dealing with the perturbations of Quintom developed in Refs.[18, 49, 70, 71], we aim to probe the time dependence of the dark energy EOS in light of WMAP3 and the combination with other tentative cosmological observations from SDSS and SNIa from the Riess "gold" sample or the SNLS observations. The background evolution and perturbations of Quintom can be identified with one normal quintessence and one phantom except for the phantom crossing point, where the natural matching condition is motivated by the case with a high-dimensional operator on the kinetic term or the two-field case and the individual sound speed for each field is assumed to be unity[18, 49, 70, 71]. In the present work we mainly focus on cases where the EOS is oscillating or with local bumps. By performing a global analysis with the Markov Chain Monte Carlo (MCMC) method, we find the current observations, in particular the WMAP3 + SDSS data combination, allow large oscillations of the EOS which can leave oscillating features on the (residual) Hubble diagram, and such oscillations are potentially detectable by future observations like SNAP. Local bumps of dark energy EOS can also leave imprints on CMB, LSS and SNIa. In cases when the bumps take place at low redshifts and the effective EOS is close to -1 , CMB and LSS observations cannot give stringent constraints on such possibilities. However, geometrical observations like (future) SNIa can possibly detect such features. On the other hand when the local bumps take place at higher redshifts beyond the detectability of SNIa, future precise observations like Gamma-ray bursts and observations of 21 cm tomography, CMB and LSS may possibly detect such features. In particular, we find that bump-like dark energy EOS on high redshifts *might* be responsible for the features of WMAP on ranges $l \sim 20 - 40$, which is interesting and deserves addressing further.

The remaining part of our paper is structured as follows: in Section II we describe the method and the data; in Section III we present our results on the determination of cosmological parameters with (WMAP3)[1, 2, 3, 4, 5], SNIa [14, 16], Sloan Digital Sky Survey 3-D power spectrum (SDSS-P(k)) [6] by global fittings using the MCMC technique; discussions and conclusions are presented in the last section.

II. METHOD AND DATA

In the parametrization of oscillating EOS one typically needs four parameters for the amplitude, center values, phase and the frequency. And in our analysis we have used

$$w = w_0 + w_1 \sin(w_2 \ln a + w_3) \quad . \quad (1)$$

The case with $w_0 = -1$ and $w_1 = 0$ corresponds to the cosmological constant.

The method we adopt is based on the publicly available Markov Chain Monte Carlo package `CosmoMC`[47, 72], which has been modified to allow for the inclusion of dark energy perturbations with EOS getting across -1 [70]. Our most

¹ For other solutions to this problem, see e.g. Refs. [41]-[45] and for a review on this issue see e.g. Ref.[46].

general parameter space is

$$\mathbf{p} \equiv (\omega_b, \omega_c, \Theta_S, \tau, w_0, w_1, w_2, w_3, n_s, \log[10^{10} A_s]) , \quad (2)$$

where $\omega_b = \Omega_b h^2$ and $\omega_c = \Omega_c h^2$ are the physical baryon and cold dark matter densities relative to critical density, Θ_S is the ratio (multiplied by 100) of the sound horizon to the angular diameter distance at decoupling, τ is the optical depth, A_s is defined as the amplitude of initial power spectrum and n_s measures the spectral index. Assuming a flat Universe motivated by inflation and basing on the Bayesian analysis, we vary the above 10 parameters and fit to the observational data with the MCMC method. We take the weak priors as: $\tau < 0.8$, $0.5 < n_s < 1.5$, $-4 < w_0 < 1$, $-10 < w_1 < 10$, $0 < w_2 < 20$, $-\pi/2 < w_3 < \pi/2$, a cosmic age tophat prior as $10 \text{ Gyr} < t_0 < 20 \text{ Gyr}$. The choice of priors on w_0, w_1, w_2, w_3 have been set to allow for spread in all of the parameters simultaneously. Furthermore, we make use of the HST measurement of the Hubble parameter $H_0 = 100h \text{ km s}^{-1} \text{ Mpc}^{-1}$ [73] by multiplying the likelihood by a Gaussian likelihood function centered around $h = 0.72$ and with a standard deviation $\sigma = 0.08$. We impose a weak Gaussian prior on the baryon and density $\Omega_b h^2 = 0.022 \pm 0.002$ (1σ) from Big Bang nucleosynthesis[74]. The bias factor of LSS has been used as a continuous parameter to give the minimum χ^2 .

In our calculations we have taken the total likelihood to be the products of the separate likelihoods of CMB, SNIa and LSS. Alternatively defining $\chi^2 = -2 \log \mathcal{L}$, we get

$$\chi_{total}^2 = \chi_{CMB}^2 + \chi_{SNIa}^2 + \chi_{LSS}^2 \quad . \quad (3)$$

In the computation of CMB we have included the three-year WMAP (WMAP3) data with the routine for computing the likelihood supplied by the WMAP team [5]. To be conservative but more robust, in the fittings to the 3D power spectrum of galaxies from the SDSS[6] we have used the first 14 bins only, which are supposed to be well within the linear regime[7]. In the calculation of the likelihood from SNIa we have marginalized over the nuisance parameter[75]. The supernova data we use are the "gold" set of 157 SNIa published by Riess *et al* in [14] and the 71 high redshift type Ia supernova discovered during the first year of the 5-year Supernova Legacy Survey (SNLS)[16] respectively. In the fittings to SNLS we have used the additional 44 nearby SNIa, as also adopted by the SNLS group[16]. Also to be conservative but more robust, we did not try to combine SNLS with the Riess sample simultaneously for cosmological parameter constraints, namely in one case for SNIa fitting we use SNLS data only and in another case the Riess sample only. For each regular calculation, we run 6 independent chains comprising of 150,000-300,000 chain elements and spend thousands of CPU hours to calculate on a cluster. The average acceptance rate is about 40%. And for the convergence test typically we get the chains satisfy the Gelman and Rubin[76] criteria where $R-1 < 0.1$.

In our study for future perspectives on features of dark energy we have used the cosmic-variance[77] limited CMB TT spectrum up to $l = 2000$. For SNIa we have used SNAP[78] simulations² and for LSS, we have adopted the LAMOST[80] simulations. In the remaining part of this paper the fiducial power law Λ CDM model adopted is as follows:

$$(\omega_b, \omega_c, h, z_r, n_s, A_s) = (0.022, 0.12, 0.7, 12, 1, 2.3 \times 10^{-9}) , \quad (4)$$

where z_r is the reionization redshift and the slightly different notations from previous Eq. (2) are due to the difference in the CAMB[81, 82] and CosmoMC[47, 72] default parameters. Such a fiducial model will be used to generate future CMB, SNIa and LSS data. In addition the illustrative figures will also be generated with such background parameters. Moreover in generating the illustrative figures on linear power spectrum of LSS we have fixed the bias factor to be unity.

The projected satellite SNAP (Supernova / Acceleration Probe) would be a space based telescope with a one square degree field of view with 1 billion pixels. It aims to increase the discovery rate for SNIa to about 2,000 per year[78]. The simulated SNIa data distribution is taken from Refs. [83, 84, 85]. As for the error, we follow the ref. [83] which takes the magnitude dispersion 0.15 and the systematic error $\sigma_{sys}(z) = 0.02 \times z/1.7$, and the whole error for each data is

$$\sigma_{mag}(z_i) = \sqrt{\sigma_{sys}^2(z_i) + \frac{0.15^2}{n_i}} , \quad (5)$$

where n_i is the number of supernova in the i 'th redshift bin.

² SNAP is one of the several candidate mission concepts for the Joint Dark Energy Mission (JDEM). Nowadays there have been many proposed dark energy surveys[79].

The Large Sky Area Multi-Object Fiber Spectroscopic Telescope (LAMOST) project as one of the National Major Scientific Projects undertaken by the Chinese Academy of Science, aims to measure $\sim 10^7$ galaxies with mean redshift $z \sim 0.2$ [80]. In the measurements of large scale matter power spectrum of galaxies there are generally two statistical errors: sample variance and shot noise. The uncertainty due to statistical effects, averaged over a radial bin Δk in Fourier space, is [86]

$$\left(\frac{\sigma_P}{P}\right)^2 = 2 \times \frac{(2\pi)^3}{V} \times \frac{1}{4\pi k^2 \Delta k} \times \left(1 + \frac{1}{\bar{n}P}\right)^2. \quad (6)$$

The initial factor of 2 is due to the real property of the density field, V is the survey volume and \bar{n} is the mean galaxy density. In our simulations for simplicity and to be conservative, we use only the linear matter power spectrum up to $k \sim 0.15 \, h \, \text{Mpc}^{-1}$.

For the cases with future cosmic variance limited CMB and LAMOST, we only show the error bars for illustrations, and a further analysis with fittings is not the aim of the present paper. For the studies on bump-like dark energy EOS, we also plot the illustrative results rather than make global fittings. And the parametrized EOS takes the following form:

$$w = w_0 + A(\ln a - \lambda)^3 \exp(-(\ln a - \lambda)^4/d). \quad (7)$$

We should point out here that the parametrization in Eq.(7) is a specific example only and there are certainly different parametrizations to illustrate the bump-like features in dark energy EOS and the resulting cosmological imprints might be different.

III. RESULTS

We start with the oscillating case. First of all in Fig.1 we delineate the illustrative imprints of oscillating dark energy equation of state (EOS) on CMB (top left), LSS (top right) and on the Hubble diagram (lower panel). In the Hubble diagram the distance modulus μ is defined as the apparent magnitude m minus the absolute magnitude M :

$$\mu \equiv m - M = 5 \lg \left(\frac{d_L}{1 \text{Mpc}} \right) + 25, \quad (8)$$

with d_L being the luminosity distance:

$$\frac{d_L}{1+z} = \int_0^z \frac{dz'}{H(z')}. \quad (9)$$

In comparison the imprints by the Λ CDM cosmology have also been displayed. The main contribution of dark energy on CMB is on the geometrical angular diameter distance to the last scattering surface. This in turn determines the locations of CMB peaks. In some cases the effects on the large scale matter power spectrum of LSS are also significant. In Fig.1 we can find for cases where $w_0 = -0.5$, the effects on CMB turn out to be most eminently modulated. This is mainly due to the fact that in such cases as w_0 deviates significantly from -1 and w has been *relatively* matter-like, the contributions to large scale CMB are significant due to the Integrated Sachs-Wolfe (ISW) effects. An oscillating EOS of dark energy can leave somewhat similar imprints as oscillating primordial spectrum, as explored in Ref. [25], although the difference is also noteworthy. We find interestingly that in cases $w_0 = -1.5$, the effects are not as large as $w_0 = -0.5$, which is in part due to the effects of dark energy perturbations and consistent with the previous analysis in Ref. [70]. The effects of dark energy on CMB (and LSS) are mainly geometrical effects and can sometimes be understood from the formula on w_{eff} [87]:

$$w_{eff} \equiv \frac{\int da \Omega(a) w(a)}{\int da \Omega(a)}. \quad (10)$$

On the other hand the Hubble diagram being displayed with the redshift, the effects of dark energy, in cases when DE dominates the Universe the EOS has oscillating features, can leave oscillations on the the Hubble diagram.

For the next step we show the results from our global fittings on the oscillating EOS in Eq.(1). In Table 1 we delineate the mean 1σ constraints on the relevant cosmological parameters using different combination of WMAP, SNIa and SDSS. Shown together are those with maximum likelihood (dubbed ML) and those which give the most eminent oscillating effects in the 2σ allowed regions (dubbed "Most" in the table). For simplicity the parameters related to bayon fractions and the primordial spectrum are not displayed, and the shown parameters are enough for

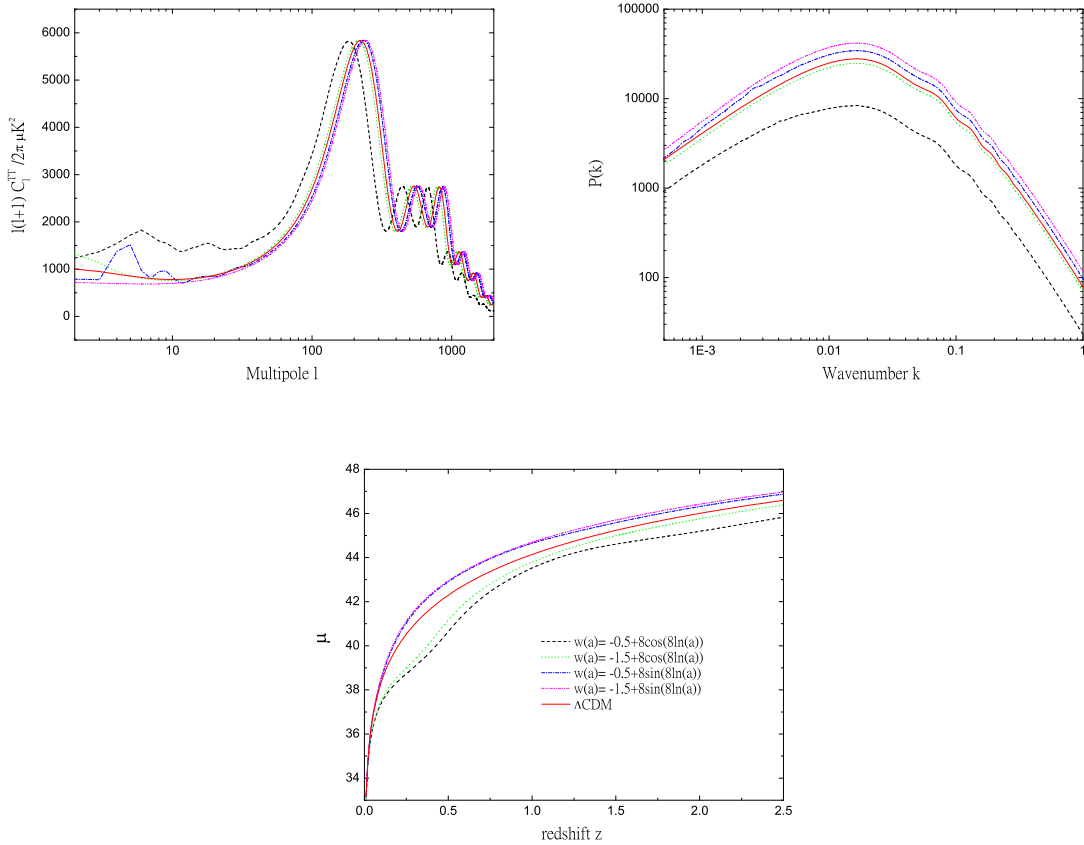


FIG. 1: Illustrative imprints of oscillating dark energy equation of state (EOS) on CMB (top left), LSS (top right) and on the Hubble diagram (lower panel) .

the study on the Hubble diagrams below. Typically in the realizations of MCMC as the cosmological parameters are not exactly gaussian distributed, the center mean values are different from the best fit cases³. We find that although the best fit cases are given by oscillating EOS, a cosmological constant ($w_0 = -1, w_1 = 0$) is well within 1σ for all the three data combinations. The accumulation of the observational data will help to break such a degeneracy. It is very interesting that w_1 is much better constrained by SNLS (together with the 44 low redshift SNIa) rather than by the Riess "gold" sample. On the other hand the background parameter H_0 is better constrained by the Riess "gold" sample. One can also find that the frequency of oscillations, w_2 , is relatively the worst constrained parameter. We will turn to this in more details in the remaining part of the present paper.

In Fig.2 we delineate the one dimensional posterior constraints on the oscillating EOS in Eq.(1), showing together some relevant background cosmological parameters. The black lines are constraints from combined analysis of WMAP3 + SDSS. The red lines are from WMAP3 + SDSS + Riess sample and the blue are from WMAP3 + SDSS + SNLS combined analysis. We can find that in some sense w_2 and w_3 are not well constrained by the current observations. As w_3 represents the phase of oscillations and the range $(-\pi/2, \pi/2)$ is the largest 1-period limit (note we have allowed w_1 to be both positive and negative), our prior on w_2 , though as large as given above, turn out to be somewhat too optimistic.

The effects are more eminent in the resulting two dimensional contours. In Fig.3 we plot the corresponding two dimensional posterior constraints. The upper panel is on the constraints from the combined analysis of WMAP3 + SDSS. The lower left panel is from WMAP3 + SDSS + Riess sample and the lower right from WMAP3 + SDSS + SNLS combined analysis.

³ More detailed discussions are available at <http://cosmocooffee.info/> .

TABLE 1. Mean 1σ constraints on cosmological parameters using different combination of WMAP, SNIa and SDSS. Shown together are those with maximum likelihood (ML) and those which give the most eminent oscillating effects within the 2σ allowed regions (Most).

	WMAP+SDSS			WMAP+SDSS+Riess			WMAP+SDSS+SNLS		
	Mean	ML	Most	Mean	ML	Most	Mean	ML	Most
w_0	$-0.805^{+0.413}_{-0.394}$	-0.465	-0.250	$-0.845^{+0.308}_{-0.222}$	-0.508	-0.450	$-0.886^{+0.283}_{-0.215}$	-0.485	-0.400
w_1	$0.874^{+2.910}_{-3.068}$	2.62	5.80	$0.609^{+1.228}_{-1.580}$	1.58	2.90	$0.303^{+0.801}_{-0.792}$	1.29	1.90
w_2	11.6 ± 5.9	18.3	11.5	$10.8^{+5.3}_{-6.0}$	12.0	10.8	$9.52^{+10.47}_{-9.49}$	8.28	9.50
w_3	$0.179^{+0.990}_{-1.730}$	-0.0707	1.5000	$-0.0446^{+0.8646}_{-1.5203}$	-0.131	1.400	$0.0831^{+0.9316}_{-1.6505}$	0.356	1.400
Ω_m	$0.345^{+0.060}_{-0.057}$	0.332	0.350	$0.308^{+0.033}_{-0.032}$	0.325	0.300	$0.288^{+0.033}_{-0.032}$	0.312	0.300
Ω_Λ	$0.655^{+0.057}_{-0.060}$	0.668	0.650	$0.692^{+0.032}_{-0.033}$	0.675	0.700	$0.712^{+0.032}_{-0.033}$	0.688	0.700
H_0	$61.8^{+5.6}_{-5.9}$	62.0	62.0	65.6 ± 3.5	63.1	65.5	$68.2^{+3.6}_{-3.7}$	62.5	68.0

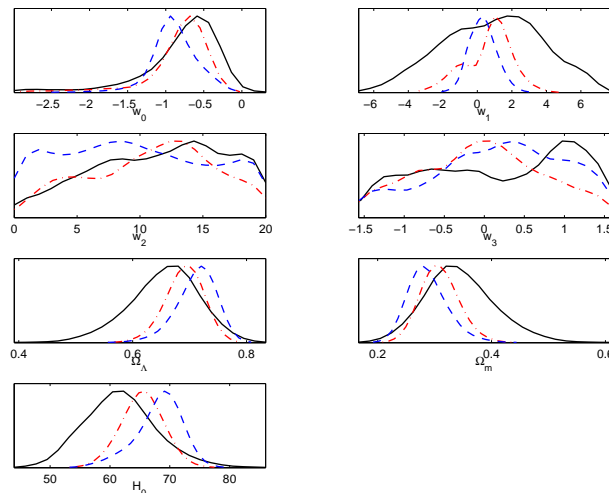


FIG. 2: One dimensional posterior constraints on the parametrized EOS: $w = w_0 + w_1 \sin(w_2 \ln a + w_3)$ and on the relevant background cosmological parameters. The black solid lines are constraints from combined analysis of WMAP3 + SDSS. The red dash-dot lines are from WMAP3 + SDSS + Riess sample and the blue dashed lines are from WMAP3 + SDSS + SNLS combined analysis .

It is understandable that in cases one or two parameters are not well constrained by the observations, changing the priors (in our case on w_2) will inevitably affect the final results. Such a feature has also appeared in previous investigations on the oscillating primordial spectrum, regardless of fitting methods one uses such as grids[88] or MCMC[89, 90]. For the grid case the problem is how small one should set the minimum grid, and there will be finer features on scales smaller than the minimum steps⁴. For our conventional cases with MCMC[18, 49, 71, 91] to get the converged results, we test the convergence of the chains by Gelman and Rubin[76] criteria and typically get R-1 to be of order 0.01, which is more conservative than the recommended value $R-1 < 0.1$. However in the present case with an oscillating EOS, in the combinations with SNLS the maximum value of R-1 is 0.04, for the combination with Riess "gold" sample, we have value: $R-1 \sim 0.1$ and for the the case with WMAP3 + SDSS we have the maximum R-1 to be 0.25 instead, although for the last case we have run much longer time for the chains. This also shows that for the case with oscillations at least for WMAP3 + SDSS our chains are not well converged. On the other hand this shows that for the current observations a large oscillation on the dark energy EOS is allowed. In Ref.[89] the authors quoted

⁴ For the grid case in the fittings to give the first year WMAP preferred running of the spectral index, in Ref. [24] in the case with an oscillating inflaton potential, the fractor-like structure is also present. Similar potentials can also lead to oscillations on the primordial spectrum, as previously investigated in Ref.[25]. And it is easily understood that in cases where the oscillations of the primordial spectrum have a large period, the resulting effects on CMB and LSS relevant scales will be running-like. Note besides inflation similar behavior also applies to the case of dark energy.

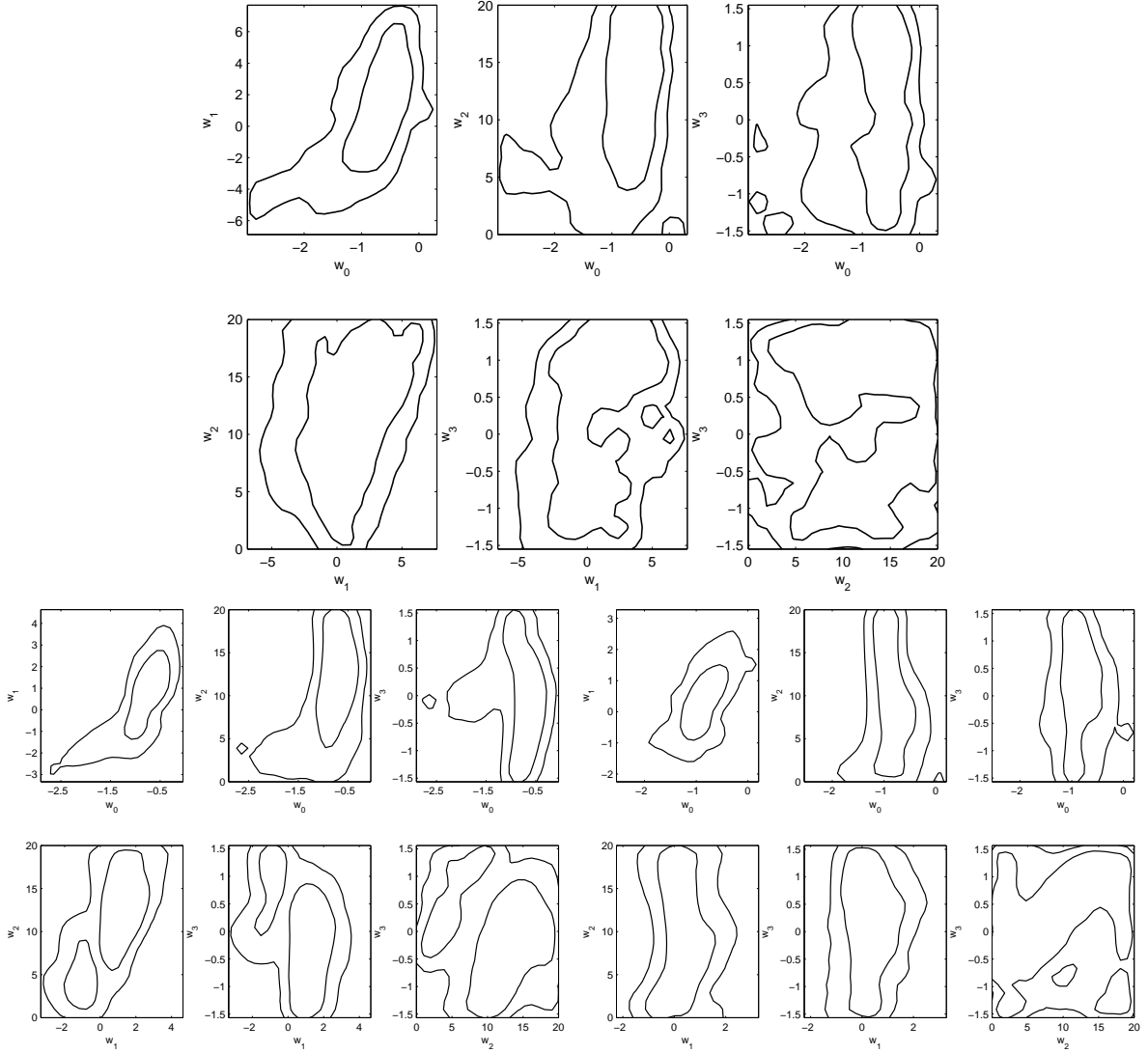


FIG. 3: Two dimensional posterior constraints on the parametrized EOS: $w = w_0 + w_1 \sin(w_2 \ln a + w_3)$ at 68% and 95% C.L. The upper panel is on the constraints from combined analysis of WMAP3 + SDSS. The lower left panel is from WMAP3 + SDSS + Riess sample and the lower right from WMAP3 + SDSS + SNLS combined analysis .

a value where $R-1 < 0.1$ (their $R-1$ is slightly different from ours) and the structures of our resulting two-dimensional figures are similar to those by Refs.[89, 90]. These have implied that in the presence of oscillations typically the current data are not good enough to well break the degeneracy among the parameters. In our case although the parameters like n_s , w_0 , Ω_{DE} , Ω_m and H_0 have already been well constrained, $R-1$ is in some cases relatively large due to the parameters w_2 and w_3 . This has in turn led to the separate likelihood spaces in the three data combinations at 68% and 95% C.L. Interestingly in the WMAP3 + SDSS + Riess sample the 1σ contours clearly separate into two different peaks in the lower three panels, resembling the contours in Ref. [89]. Such a behavior is less eminent in the WMAP3 + SDSS + SNLS sample, which nevertheless does exist in the $w_2 - w_3$ contour. We should point out that given the priors and the $R-1$ value specified above, our results are robust. In Fig.4 we delineate the resulting posterior 1σ constraints on the low-redshift behavior of the oscillating EOS, with the three different data combinations. The red lines are given by the mean center values as shown in Table 1 and the blue dashes lines are the 1σ allowed regions. The green dashed lines are the illustrative 1σ explored regions by future SNAP[78]. Thus future SNIa observations like SNAP can help significantly to break the degeneracy, and in some sense detect such oscillating features of dark energy EOS.

In Fig.5 we delineate the corresponding imprints on the residue Hubble diagram (upper panels) and the Hubble diagram (lower panels). In the left panels, the lines dubbed "Osc" are given by the best fit values WMAP3 + SDSS,

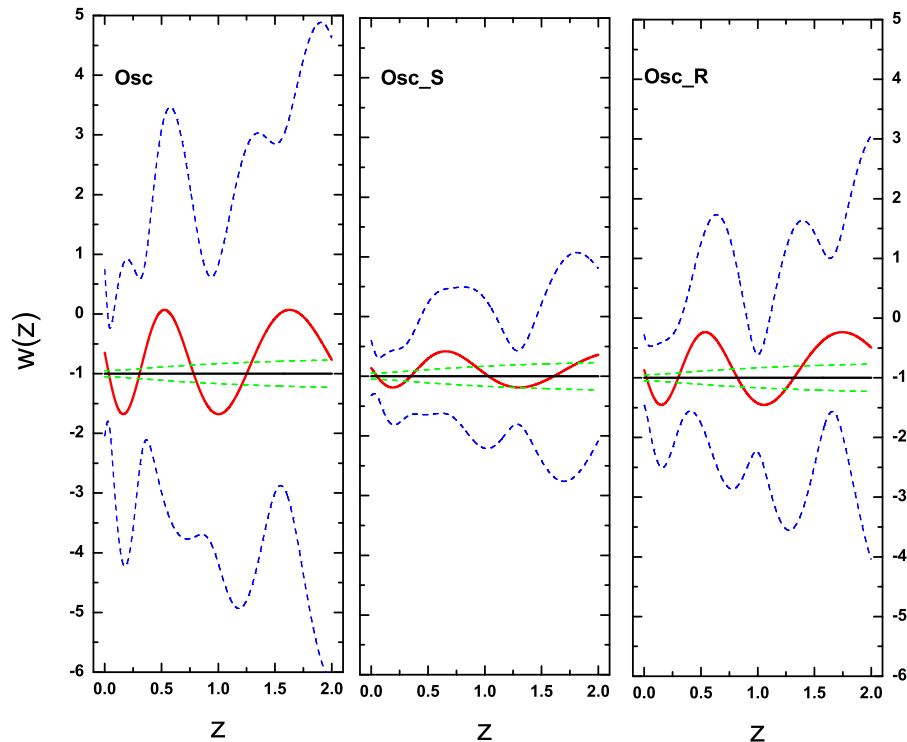


FIG. 4: Resulting posterior constraints on the low-redshift behavior of the parametrized EOS: $w = w_0 + w_1 \sin(w_2 \ln a + w_3)$. The red lines are given by the mean center values as shown in Table 1 and the outside blue dashed lines are the 1σ allowed regions by WMAP3 + SDSS (left), WMAP3 + SDSS + SNLS (center) and WMAP3 + SDSS + Riess sample (right). The inside green dashed lines are the illustrative 1σ explored regions by future SNAP.

the underlined "S" is by WMAP3 + SDSS + SNLS and "R" by WMAP3 + SDSS + Riess sample. The right panels show the corresponding cases where within the 2σ allowed regions the oscillating effects are relatively eminent. Same as the above conventions in the upper panels the blue lines dubbed "SNAP" illustrate the detectability of future SNAP[78]. It is noteworthy that the combination with SNLS gives relatively the most stringent constraints. We can find that for the case with WMAP + SDSS only, a larger oscillation is allowed and there are some oscillating features on the (residue) Hubble diagram. And the effects of the "Most" case in Table 1 are more eminent, which could be possibly detected even by the CURRENTLY ONGOING SNIa observations. In the cases combined with Riess "gold" sample or with SNLS, the oscillating effects are less eminent. Nevertheless, oscillations are still present and in large areas of the parameter spaces, SNAP will be able to detect such features⁵.

Now we turn to the studies on the local bump-like features of dark energy EOS. It is physically intuitive that dark energy EOS might not be exactly periodic, instead it could be semi-periodic or even with features on some specific redshifts. The parametrization adopted in Eq. (7) ($w = w_0 + A(\ln a - \lambda)^3 \exp(-(\ln a - \lambda)^4/d)$) can accommodate constant EOS in cases where $A = 0$. λ determines the locations of bumps, d determines the width and A determines the amplitudes of the bumps. One can easily understand that at the point $\ln a = \lambda$ we have $w = w_0$ and for $\ln a < \lambda$ (high redshifts) there will be a trough and for $\ln a > \lambda$ (low redshifts) there will be a peak (this happens only in cases

⁵ In some sense in Table 1 for the "Most" case by WMAP + SDSS combination only, the relevant parameter space will get relatively stringently constrained by combinations with SNLS or with Riess "gold" sample. However given the possible discrepancies between SNLS and the Riess sample, which has been somewhat illustrated in Ref. [1], currently ongoing SNIa observations can in some sense detect the (semi)-oscillating features in dark energy EOS as allowed by WMAP + SDSS combination.

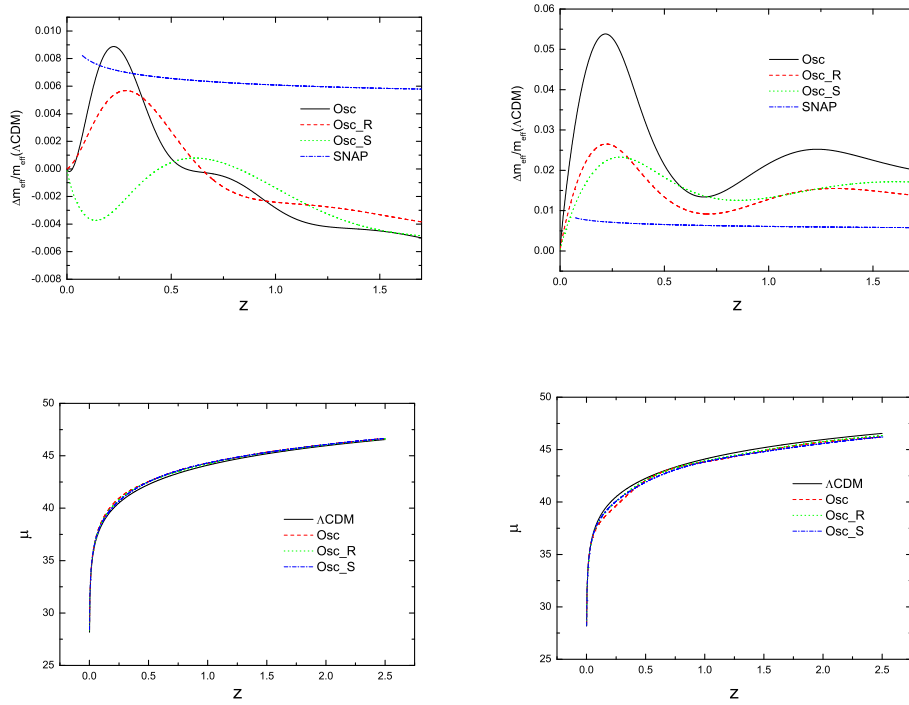


FIG. 5: Resulting imprints of the parametrized EOS: $w = w_0 + w_1 \sin(w_2 \ln a + w_3)$ on the residue Hubble diagram (upper panels) and the Hubble diagram (lower panels). In the left panels, the lines dubbed "Osc" are given by the best fit values WMAP3 + SDSS, the underlined "S" is by WMAP3 + SDSS + SNLS and "R" by WMAP3 + SDSS + Riess sample. The right panels show the corresponding cases where within the 2σ allowed regions the oscillating effects are relatively eminent. In the upper panels the blue lines dubbed "SNAP" illustrate the detectability of future SNAP.

where $\lambda < 0$, which is the region of our interest). And on very high redshifts where $\ln a \ll \lambda$ the second term will get damped exponentially and w approaches the value of w_0 . For simplicity and in the illustrative study here we fix $w_0 = -1$.

Firstly we consider the cases where the bump takes place at low redshifts which can be detectable by (future) SNIa observations. In Fig.6 we delineate the imprints of bump-like dark energy EOS on the (residual) Hubble diagram, dark energy density fractions (left) and the corresponding effects on CMB and LSS (right). We have chosen $A = 2 \times 10^7$, $\lambda = -0.03$ and $d = 10^{-7}$ for the first illustration. From Fig.6 we can find that for such a specific choice of parameters the effects on CMB are indistinguishable from the corresponding Λ CDM model beyond cosmic variance, and nor can LSS tell one (bump-like) from the other (Λ CDM). It is understandable that in such a case as the effects of the peak and trough somewhat cancel out in the contributions to w_{eff} defined in Eq. (10), the effects on CMB and LSS would then be *almost* indistinguishable from the Λ CDM case, and the results are consistent with those in Refs.[70, 87]. In such a case, observations with geometric constraints on the redshift "tomography" will be of great importance to break such a degeneracy. The resulting (residual) Hubble diagrams are different from the Λ CDM model, and observations like SNAP can possibly detect such features.

Although SNIa in some sense makes the only direct detection of dark energy, it is believed that due to some unavoidable effects like by dust the redshifts probed by SNIa cannot be too high, and for example in SNAP simulations one typically takes $z \leq 1.7$. In cases when the bump-like features take place at higher redshifts, we cannot expect to probe such features with even future SNAP observations. On the other hand as the current observations are consistent with a Λ -like dark energy, typically we cannot hope dark energy will be non-negligible in epochs far before the matter-radiation equality epoch, although such a possibility remains (for relevant studies see e.g. [92, 93]). On the other hand with our parametrized EOS given in Eq. (7) we cannot expect dark energy component to be significant

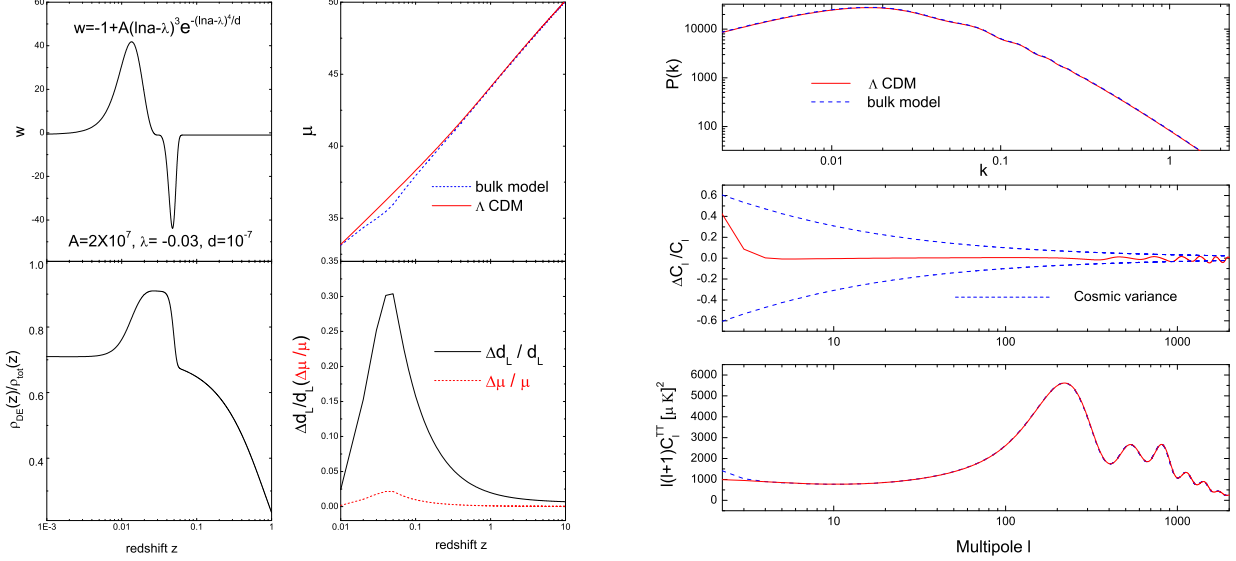


FIG. 6: Imprints of bump-like dark energy EOS (denoted by "bulk model") on the (residual) Hubble diagram, dark energy density fractions (left) and the corresponding effects on CMB and LSS (right), shown together with the imprints by the Λ CDM model. The bump takes place at low redshifts which can be detectable by (future) SNIa observations. The effects on CMB are indistinguishable from the corresponding Λ CDM model beyond cosmic variance, and nor can LSS tell one (bump-like) from the other (Λ CDM).

on very high redshifts, especially for cases where $w_0 = -1$ ⁶. Under such a circumstance we take the locations of bumps to be slightly larger than $z = 2$: in one case $\lambda = -1.5$ and in another case $\lambda = -1.8$. These correspond to $z \simeq 3.5$ and 5.0 respectively where $\ln a = \lambda$. For both of the cases we have fixed $A = 6 \times 10^5$ and $d = 10^{-5}$. In Fig.7 we show the imprints of bump-like dark energy EOS on CMB, LSS (right panels), on dark energy density fractions and on the residual Hubble diagram (left panels). The bumps take place at high redshifts which cannot be detectable by (future) SNIa observations. On the other hand, observations of Gamma-ray bursts (GRB) can probe relatively higher redshifts than SNIa[94, 95, 96], with the accumulations of GRB events as by SWIFT and better understandings on the systematics one is hopefully able to detect such features through geometric observations on the Hubble diagrams. Moreover observations like the 21 cm tomography [97, 98, 99, 100] are potentially able to give almost a large number of independent samples compared with CMB and LSS observations[98], features of bump-like dark energy EOS on intermediate redshifts are promisingly detected by observations of the 21 cm tomography. In the right panels of Fig.7 we find dramatically that bump-like features are possibly detectable by cosmic variance limited CMB (e.g. WMAP3[1, 2, 3, 4, 5]) and LAMOST[80]. Part of the reason lies on the fact that with a different width and a higher redshift compared with the previous example in Fig.6, here the energy density fraction $\Omega_{DE}(a)$ increases and decreases rapidly and the magnitude of the peak value of $\Omega_{DE}(a)$ is somewhat lower, the asymmetric shapes of the peak and trough cannot compensate thoroughly to give w_{eff} close to -1 . In fact one can find for our parametrization given in Eq. (7) one will typically get $w_{eff} > -1$ and in cases with larger $-\lambda$ the deviation of w_{eff} from -1 can be larger, which will also lead to some shifts on CMB peaks, as shown in Fig.7. It is noteworthy to point out that both the first year WMAP and WMAP3 show some local glitches out of cosmic variance at $l \sim 20 - 40$. In our case of Fig.7 there are also some relevant features on such scales and this deserves further investigations. While such features can be affected by different foreground analysis and so forth[101, 102, 103], it is theoretically possible that the features of WMAP TT on scales $l \sim 20 - 40$ are due to some bump-like features of dark energy EOS, or some semi-oscillations. Note here we have fixed the background parameters rather than performing a global analysis, and in cases we take into account the parameter degeneracies the detectability of the observations would typically get

⁶ This is however, still possible given some fine tunings on the remaining parameters in Eq. (7), which will not be explored by the current paper.

weaker. On the other hand we can expect that in the global analysis when all of the parameters (including the bias factor) can vary, the observations can give constraints or detect the signatures where the amplitudes of bumps are even higher than the examples listed above.

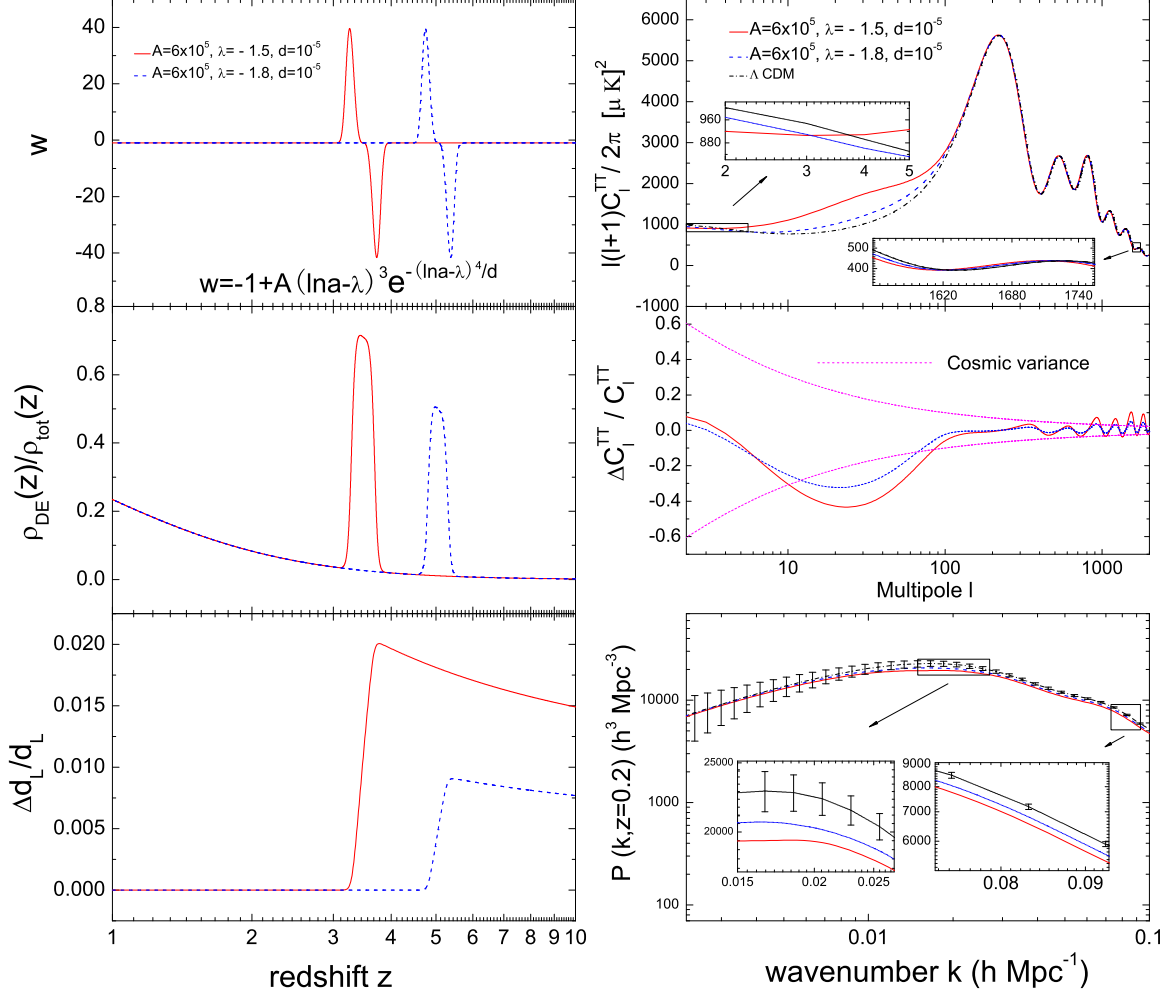


FIG. 7: Imprints of bump-like dark energy EOS on CMB, LSS (right panels), on dark energy density fractions and on the residual Hubble diagram (left panels). The bumps take place at high redshifts which cannot be detectable by (future) SNIa observations. On the other hand, cosmic variance limited CMB (e.g. WMAP3) and LAMOST[80] are possible to detect such features. Note here we have not performed a global analysis and did not take into account the parameter degeneracies.

IV. DISCUSSION AND CONCLUSION

We should point that in all our three data combinations, a large area of oscillating Quintom where the EOS of dark energy gets across -1 during time evolutions are allowed by the current observations, which is different from the previous case in Ref.[50] and from the case in Ref. [53]. Moreover contrary to Refs.[50, 53], oscillating Quintom displays the distinctive feature that due to the average effects on the regions of EOS where $w > -1$ and $w < -1$, the quantity w_{eff} can be very close to -1 . Oscillating Quintom-like dark energy, where the unification of two epochs of accelerated expansions can be realized and the coincidence problem can be solved[51], proves to be a good fit to current

cosmology. We should stress again that resembling the oscillating primordial spectrum case[89], the not good enough convergence of oscillating dark energy EOS is inevitable in the light of the current observations. In the WMAP + SDSS allowed parameter space there are areas with significant oscillations, which implies that the CURRENTLY ONGOING SNIa observations may detect such oscillating or semi-oscillating features on the (residual) Hubble diagram. Moreover while oscillating features on CMB might be explained by both oscillating primordial spectrum and oscillations in dark energy EOS, the oscillating features on the Hubble diagram cannot be due to features in the primordial spectrum, but by oscillating EOS. Local bumps of dark energy EOS may leave some distinctive imprints on CMB, LSS and SNIa. The bumps are potentially detectable by geometrical observations like SNIa and GRB. Future observations of 21 cm tomography open a very promising window to detect/exclude such features. LSS measurements like LAMOST and cosmic variance limited CMB may also detect such features. In particular, bump-like dark energy EOS on high redshifts *might* be responsible for the features of WMAP on ranges $l \sim 20 - 40$, which is interesting and deserves addressing further.

Given the fact that currently we know relatively very little on theoretical aspects of dark energy, observing dynamical dark energy is currently the most important aspect of dark energy study. On the observational probes typically one needs some parametrizations on the form of dark energy EOS. While using some specific forms of parametrizations one often takes the risks of getting biased (see e.g. [104]), investigations towards unbiased probe of DE[105, 106, 107] in light of all the available cosmological observations still need further developments. On the other hand some of the parametrizations are in some sense well motivated (see e.g. [104]), and in fittings starting with parametrized EOS one typically has larger ν (number of data minus the number of parameters) and hence gets better constraints on dark energy. With the accumulations of observational data poor parametrizations will get ruled out and in this sense parametrized study of dark energy provides a complementary study of the non-parametric probes. As from any quintessence-like or phantom-like EOS which do not get across -1 one can reconstruct the dark energy potential[108], any parametrizations of non-Quintom-like EOS correspond to some specific forms of quintessence/phantom potentials⁷ and hence such parametrizations are somewhat well motivated. Bump-like EOS which do not get across -1 also correspond to some specific DE potentials which can be straightforwardly worked out. Similarly for (semi-)oscillating EOS which do not get across -1 one can work out the corresponding DE potentials. In cases with bumps described in Eq. (7) and with oscillations in Eq. (1), one cannot simply reconstruct the potentials of DE due to the distinctive nature of Quintom[54, 70]. However this remains possible for example the models with high derivatives [65, 67] and in the framework with modified gravity[56, 109, 110, 111, 112, 113].

Acknowledgments: We acknowledge the use of the Legacy Archive for Microwave Background Data Analysis (LAMBD A). Support for LAMBD A is provided by the NASA Office of Space Science. We have performed our numerical analysis on the Shanghai Supercomputer Center (SSC). We used a modified version of CAMB[81, 82] which is based on CMBFAST[114, 115]. We are grateful to Hiranya Peiris, Yunsong Piao and Lifan Wang for discussions related to this project. We thank Xuelei Chen, Yaoquan Chu and Long-long Feng for discussions on LAMOST. We thank Sarah Bridle, Peihong Gu, Steen Hannestad, Antony Lewis, Mingzhe Li, Yongzhong Xu, Jun'ichi Yokoyama, Max Tegmark and Penjie Zhang for helpful discussions. B. F. would like to thank the hospitalities of IHEP during his visit to Beijing. This work is supported in part by National Natural Science Foundation of China under Grant Nos. 90303004, 10533010 and 19925523 and by Ministry of Science and Technology of China under Grant No. NKBRSF G19990754. B. F. is supported by the JSPS fellowship program.

-
- [1] D. N. Spergel *et al.*, arXiv:astro-ph/0603449.
 - [2] L. Page *et al.*, arXiv:astro-ph/0603450;
 - [3] G. Hinshaw *et al.*, arXiv:astro-ph/0603451;
 - [4] N. Jarosik *et al.*, arXiv:astro-ph/0603452.
 - [5] Available from <http://lambda.gsfc.nasa.gov/product/map/current/>.
 - [6] M. Tegmark *et al.* [SDSS Collaboration], *Astrophys. J.* **606**, 702 (2004) [arXiv:astro-ph/0310725].
 - [7] M. Tegmark *et al.* [SDSS Collaboration], *Phys. Rev. D* **69**, 103501 (2004) [arXiv:astro-ph/0310723].
 - [8] S. Weinberg, *Rev. Mod. Phys.* **61**, 1 (1989).
 - [9] I. Zlatev, L. M. Wang and P. J. Steinhardt, *Phys. Rev. Lett.* **82**, 896 (1999) [arXiv:astro-ph/9807002].
 - [10] R. D. Peccei, J. Sola and C. Wetterich, *Phys. Lett. B* **195**, 183 (1987); C. Wetterich, *Nucl. Phys. B* **302**, 668 (1988); B. Ratra and P. J. E. Peebles, *Phys. Rev. D* **37**, 3406 (1988).
 - [11] A. G. Riess *et al.* [Supernova Search Team Collaboration], *Astron. J.* **116**, 1009 (1998) [arXiv:astro-ph/9805201].

⁷ In cases where $w > 1$ they correspond to quintessence with negative potentials.

- [12] S. Perlmutter *et al.* [Supernova Cosmology Project Collaboration], *Astrophys. J.* **517**, 565 (1999) [arXiv:astro-ph/9812133].
- [13] J. L. Tonry *et al.* [Supernova Search Team Collaboration], *Astrophys. J.* **594**, 1 (2003) [arXiv:astro-ph/0305008].
- [14] A. G. Riess *et al.* (Supernova Search Team Collaboration), *Astrophys. J.* **607**, 665 (2004) [arXiv:astro-ph/0402512].
- [15] A. Clocchiatti *et al.* (the High Z SN Search Collaboration), astro-ph/0510155.
- [16] P. Astier *et al.*, *Astron. Astrophys.* **447**, 31 (2006) [arXiv:astro-ph/0510447].
- [17] U. Seljak, A. Slosar and P. McDonald, arXiv:astro-ph/0604335.
- [18] G. B. Zhao, J. Q. Xia, B. Feng and X. Zhang, arXiv:astro-ph/0603621.
- [19] Y. Wang and P. Mukherjee, arXiv:astro-ph/0604051.
- [20] C. L. Bennett *et al.*, *Astrophys. J. Suppl.* **148**, 1 (2003) [arXiv:astro-ph/0302207].
- [21] D. N. Spergel *et al.* [WMAP Collaboration], *Astrophys. J. Suppl.* **148**, 175 (2003) [arXiv:astro-ph/0302209].
- [22] H. V. Peiris *et al.*, *Astrophys. J. Suppl.* **148**, 213 (2003) [arXiv:astro-ph/0302225].
- [23] e.g. C. R. Contaldi, M. Peloso, L. Kofman and A. Linde, *JCAP* **0307**, 002 (2003); B. Feng and X. Zhang, *Phys. Lett. B* **570**, 145 (2003); Q. G. Huang and M. Li, *JCAP* **0311**, 001 (2003) [arXiv:astro-ph/0308458]; M. Yamaguchi and J. Yokoyama, *Phys. Rev. D* **70** (2004) 023513; Y. S. Piao, B. Feng and X. m. Zhang, *Phys. Rev. D* **69**, 103520 (2004) [arXiv:hep-th/0310206]; Y. S. Piao, S. Tsujikawa and X. m. Zhang, *Class. Quant. Grav.* **21**, 4455 (2004) [arXiv:hep-th/0312139]; Y. S. Piao, *Phys. Rev. D* **71**, 087301 (2005) [arXiv:astro-ph/0502343]; B. A. Bassett, S. Tsujikawa and D. Wands, arXiv:astro-ph/0507632.
- [24] B. Feng, M. z. Li, R. J. Zhang and X. m. Zhang, *Phys. Rev. D* **68**, 103511 (2003) [arXiv:astro-ph/0302479].
- [25] X. Wang, B. Feng, M. Li, X. L. Chen and X. Zhang, *Int. J. Mod. Phys. D* **14**, 1347 (2005) [arXiv:astro-ph/0209242].
- [26] T. Moroi and T. Takahashi, *Phys. Rev. Lett.* **92**, 091301 (2004) [arXiv:astro-ph/0308208].
- [27] B. Feng, X. Gong and X. Wang, *Mod. Phys. Lett. A* **19**, 2377 (2004) [arXiv:astro-ph/0301111].
- [28] M. Viel, M. G. Haehnelt and A. Lewis, arXiv:astro-ph/0604310.
- [29] L. A. Kofman, A. D. Linde, A. A. Starobinsky, *Phys. Lett. B* **157**, 361 (1985).
- [30] A. A. Starobinsky, *JETP Lett.* **55**, 489 (1992) [*Pisma Zh. Eksp. Teor. Fiz.* **55**, 477 (1992)].
- [31] J. A. Adams, G. G. Ross and S. Sarkar, *Nucl. Phys. B* **503**, 405 (1997) [arXiv:hep-ph/9704286].
- [32] J. Lesgourgues, D. Polarski and A. A. Starobinsky, *Mon. Not. Roy. Astron. Soc.* **297**, 769 (1998) [arXiv:astro-ph/9711139].
- [33] D. J. H. Chung, E. W. Kolb, A. Riotto and I. I. Tkachev, *Phys. Rev. D* **62**, 043508 (2000) [arXiv:hep-ph/9910437].
- [34] L. M. Wang and M. Kamionkowski, *Phys. Rev. D* **61**, 063504 (2000) [arXiv:astro-ph/9907431].
- [35] J. Lesgourgues, *Nucl. Phys. B* **582**, 593 (2000) [arXiv:hep-ph/9911447].
- [36] L. M. Griffiths, J. Silk and S. Zaroubi, *Mon. Not. Roy. Astron. Soc.* **324**, 712 (2001) [arXiv:astro-ph/0010571].
- [37] S. Hannestad, S. H. Hansen and F. L. Villante, *Astropart. Phys.* **16**, 137 (2001) [arXiv:astro-ph/0012009].
- [38] J. Barriga, E. Gaztanaga, M. G. Santos and S. Sarkar, *Mon. Not. Roy. Astron. Soc.* **324**, 977 (2001) [arXiv:astro-ph/0011398].
- [39] M. Gramann and G. Hutsi, *Mon. Not. Roy. Astron. Soc.* **327**, 538 (2001) [arXiv:astro-ph/0102466].
- [40] M. Kamionkowski and A. R. Liddle, *Phys. Rev. Lett.* **84**, 4525 (2000) [arXiv:astro-ph/9911103]; A. R. Zentner and J. S. Bullock, *Phys. Rev. D* **66**, 043003 (2002) [arXiv:astro-ph/0205216].
- [41] D. N. Spergel and P. J. Steinhardt, *Phys. Rev. Lett.* **84**, 3760 (2000) [arXiv:astro-ph/9909386].
- [42] B. D. Wandelt, *et al.* *Proceedings of Dark Matter 2000*, arXiv:astro-ph/0006344.
- [43] M. Kaplinghat, L. Knox and M. S. Turner, *Phys. Rev. Lett.* **85**, 3335 (2000) [arXiv:astro-ph/0005210].
- [44] W. B. Lin, D. H. Huang, X. Zhang and R. H. Brandenberger, *Phys. Rev. Lett.* **86**, 954 (2001) [arXiv:astro-ph/0009003].
- [45] P. Bode, J. P. Ostriker and N. Turok, *Astrophys. J.* **556**, 93 (2001) [arXiv:astro-ph/0010389].
- [46] A. Tasitsiomi, *Int. J. Mod. Phys. D* **12**, 1157 (2003) [arXiv:astro-ph/0205464].
- [47] A. Lewis and S. Bridle, *Phys. Rev. D* **66**, 103511 (2002) [arXiv:astro-ph/0205436].
- [48] P. J. E. Peebles and A. Vilenkin, *Phys. Rev. D* **59**, 063505 (1999) [arXiv:astro-ph/9810509].
- [49] J. Q. Xia, G. B. Zhao, B. Feng and X. Zhang, arXiv:astro-ph/0603393.
- [50] S. Dodelson, M. Kaplinghat and E. Stewart, *Phys. Rev. Lett.* **85**, 5276 (2000).
- [51] B. Feng, M. Li, Y. S. Piao and X. Zhang, *Phys. Lett. B* **634**, 101 (2006) [arXiv:astro-ph/0407432].
- [52] G. Barenboim and J. D. Lykken, *Phys. Lett. B* **633**, 453 (2006) [arXiv:astro-ph/0504090].
- [53] For an interesting relevant study see G. Barenboim, O. Mena and C. Quigg, *Phys. Rev. D* **71**, 063533 (2005) [arXiv:astro-ph/0412010].
- [54] B. Feng, X. L. Wang and X. M. Zhang, *Phys. Lett. B* **607**, 35 (2005) [arXiv:astro-ph/0404224].
- [55] S. Weinberg, *Phys. Rev. Lett.* **59**, 2607 (1987).
- [56] G. R. Dvali, G. Gabadadze and M. Porrati, *Phys. Lett. B* **485**, 208 (2000) [arXiv:hep-th/0005016].
- [57] K. Koyama, *Phys. Rev. D* **72**, 123511 (2005) [arXiv:hep-th/0503191].
- [58] For an interesting relevant study see J. Yokoyama, *Phys. Rev. Lett.* **88**, 151302 (2002) [arXiv:hep-th/0110137].
- [59] For a recent review see A. Vilenkin, arXiv:astro-ph/0605242.
- [60] For a review see E. J. Copeland, M. Sami and S. Tsujikawa, arXiv:hep-th/0603057.
- [61] e.g. H. Wei and R.-G. Cai, arXiv:hep-th/0501160; R.-G. Cai, H.-S. Zhang and A. Wang, arXiv:hep-th/0505186; A. A. Andrianov, F. Cannata and A. Y. Kamenshchik, arXiv:gr-qc/0505087; X. Zhang, arXiv:astro-ph/0504586; Q. Guo and R.-G. Cai, arXiv:gr-qc/0504033; B. McInnes, *Nucl. Phys. B* **718**, 55 (2005); I. Y. Aref'eva, A. S. Koshelev, and S. Yu. Vernov, arXiv:astro-ph/0507067; C. G. Huang and H. Y. Guo, arXiv:astro-ph/0508171; W. Zhao, arXiv:astro-ph/0604460; J. Grande, J. Sola and H. Stefancic, arXiv:gr-qc/0604057; L. P. Chimento and R. Lazkoz, arXiv:astro-ph/0604090; F. Cannata and A. Y. Kamenshchik, arXiv:gr-qc/0603129; R. Lazkoz and G. Leon, arXiv:astro-ph/0602590; B. Feng,

- arXiv:astro-ph/0602156; H. Stefancic, arXiv:astro-ph/0511316; L. Perivolaropoulos, arXiv:astro-ph/0601014.
- [62] T. Chiba, T. Okabe and M. Yamaguchi, Phys. Rev. D **62** (2000) 023511 [arXiv:astro-ph/9912463]; C. Armendariz-Picon, V. F. Mukhanov and P. J. Steinhardt, Phys. Rev. Lett. **85**, 4438 (2000) [arXiv:astro-ph/0004134].
- [63] R. R. Caldwell, Phys. Lett. B **545**, 23 (2002) [arXiv:astro-ph/9908168].
- [64] Z. K. Guo, Y. S. Piao, X. M. Zhang and Y. Z. Zhang, Phys. Lett. B **608**, 177 (2005) [arXiv:astro-ph/0410654].
- [65] M. z. Li, B. Feng and X. m. Zhang, JCAP **0512**, 002 (2005) [arXiv:hep-ph/0503268].
- [66] X. F. Zhang, H. Li, Y. S. Piao and X. M. Zhang, Mod. Phys. Lett. A **21**, 231 (2006) [arXiv:astro-ph/0501652].
- [67] X. F. Zhang and T. Qiu, arXiv:astro-ph/0603824.
- [68] J. Q. Xia, B. Feng and X. M. Zhang, Mod. Phys. Lett. A **20**, 2409 (2005) [arXiv:astro-ph/0411501].
- [69] E. V. Linder, Astropart. Phys. **25**, 167 (2006) [arXiv:astro-ph/0511415].
- [70] G. B. Zhao, J. Q. Xia, M. Li, B. Feng and X. Zhang, Phys. Rev. D **72**, 123515 (2005) [arXiv:astro-ph/0507482].
- [71] J. Q. Xia, G. B. Zhao, B. Feng, H. Li and X. Zhang, Phys. Rev. D **73**, 063521 (2006) [arXiv:astro-ph/0511625].
- [72] Available from <http://cosmologist.info>.
- [73] W. L. Freedman *et al.*, Astrophys. J. **553**, 47 (2001) [arXiv:astro-ph/0012376].
- [74] S. Burles, K. M. Nollett and M. S. Turner, Astrophys. J. **552**, L1 (2001) [arXiv:astro-ph/0010171].
- [75] For details see e.g. E. Di Pietro and J. F. Claeskens, Mon. Not. Roy. Astron. Soc. **341**, 1299 (2003), [arXiv:astro-ph/0207332].
- [76] A. Gelman and D. Rubin, Statistical Science **7**, 457 (1992).
- [77] J. R. Bond and G. Efstathiou, Mon. Not. Roy. Astron. Soc. **226**, 655 (1987).
- [78] Available at <http://snap.lbl.gov>.
- [79] See e.g. A. Crotts *et al.*, arXiv:astro-ph/0507043; T. Abbott *et al.* [Dark Energy Survey Collaboration], arXiv:astro-ph/0510346.
- [80] Available at <http://www.lamost.org/>.
- [81] A. Lewis, A. Challinor and A. Lasenby, Astrophys. J. **538**, 473 (2000) [arXiv:astro-ph/9911177].
- [82] Available at <http://camb.info>.
- [83] A. G. Kim, E. V. Linder, R. Miquel and N. Mostek, Mon. Not. Roy. Astron. Soc. **347**, 909 (2004) [arXiv:astro-ph/0304509].
- [84] C. Yeche, A. Ealet, A. Refregier, C. Tao, A. Tilquin, J. M. Virey and D. Yvon, arXiv:astro-ph/0507170.
- [85] H. Li, B. Feng, J. Q. Xia and X. Zhang, Phys. Rev. D **73**, 103503 (2006) [arXiv:astro-ph/0509272].
- [86] H. A. Feldman, N. Kaiser and J. A. Peacock, Astrophys. J. **426**, 23 (1994) [arXiv:astro-ph/9304022].
- [87] e.g. L. M. Wang, R. R. Caldwell, J. P. Ostriker and P. J. Steinhardt, Astrophys. J. **530**, 17 (2000) [arXiv:astro-ph/9901388].
- [88] O. Elgaroy and S. Hannestad, Phys. Rev. D **68**, 123513 (2003) [arXiv:astro-ph/0307011].
- [89] T. Okamoto and E. A. Lim, Phys. Rev. D **69**, 083519 (2004) [arXiv:astro-ph/0312284].
- [90] R. Easther, W. H. Kinney and H. Peiris, JCAP **0505**, 009 (2005) [arXiv:astro-ph/0412613].
- [91] B. Feng, M. Li, J. Q. Xia, X. Chen and X. Zhang, arXiv:astro-ph/0601095.
- [92] M. Malquarti and A. R. Liddle, Phys. Rev. D **66**, 023524 (2002) [arXiv:astro-ph/0203232].
- [93] W. Wang and B. Feng, Chin. J. Astron. Astrophys. **3**, 105 (2003) [arXiv:astro-ph/0508139].
- [94] K. Takahashi, M. Oguri, K. Kotake and H. Ohno, arXiv:astro-ph/0305260.
- [95] Z. G. Dai, E. W. Liang and D. Xu, Astrophys. J. **612**, L101 (2004) [arXiv:astro-ph/0407497].
- [96] D. Hooper and S. Dodelson, arXiv:astro-ph/0512232.
- [97] G. B. Field, Astrophys. J. **129**, 536 (1959).
- [98] A. Loeb and M. Zaldarriaga, Phys. Rev. Lett. **92**, 211301 (2004) [arXiv:astro-ph/0312134].
- [99] X. L. Chen and J. Miralda-Escude, Astrophys. J. **602**, 1 (2004) [arXiv:astro-ph/0303395].
- [100] e.g. U. L. Pen, X. P. Wu and J. Peterson, arXiv:astro-ph/0404083.
- [101] See also A. Slosar, U. Seljak and A. Makarov, “Exact likelihood evaluations and foreground marginalization in low resolution WMAP data,” Phys. Rev. D **69**, 123003 (2004) [arXiv:astro-ph/0403073].
- [102] A. de Oliveira-Costa and M. Tegmark, Phys. Rev. D **74**, 023005 (2006) [arXiv:astro-ph/0603369].
- [103] H. K. Eriksen *et al.*, “A re-analysis of the three-year WMAP temperature power spectrum and arXiv:astro-ph/0606088.
- [104] B. A. Bassett, P. S. Corasaniti and M. Kunz, Astrophys. J. **617**, L1 (2004) [arXiv:astro-ph/0407364].
- [105] D. Huterer and G. Starkman, Phys. Rev. Lett. **90**, 031301 (2003) [arXiv:astro-ph/0207517].
- [106] Y. Wang and M. Tegmark, Phys. Rev. D **71**, 103513 (2005) [arXiv:astro-ph/0501351].
- [107] J. Simon, L. Verde and R. Jimenez, Phys. Rev. D **71**, 123001 (2005) [arXiv:astro-ph/0412269].
- [108] A. Lewis, CAMB notes.
- [109] M. Morikawa, Astrophys. J. **362**, L 37 (1990); Astrophys. J. **369**, 20 (1991).
- [110] V. Sahni and Y. Shtanov, JCAP **0311**, 014 (2003) [arXiv:astro-ph/0202346].
- [111] L. Perivolaropoulos, Phys. Rev. D **67**, 123516 (2003) [arXiv:hep-ph/0301237].
- [112] H. Stefancic, Eur. Phys. J. C **36**, 523 (2004) [arXiv:astro-ph/0312484].
- [113] L. Perivolaropoulos, JCAP **0510**, 001 (2005) [arXiv:astro-ph/0504582].
- [114] U. Seljak and M. Zaldarriaga, Astrophys. J. **469**, 437 (1996) [arXiv:astro-ph/9603033].
- [115] Available at <http://cmbfast.org/>.